Summing Logarithmic Expansions for Elliptic Equations in Multiply-Connected Domains with Small Holes

Michèle S. Titcombe and Michael J. Ward[1]
Department of Mathematics
University of British Columbia
Vancouver, Canada

Abstract

Elliptic problems in a two-dimensional domain containing one or several small holes is studied asymptotically in the limit of small hole radius ε. As a result of the perturbation, the asymptotic solution to this class of problems contains an infinite logarithmic expansion in powers of $-1/\log\varepsilon$. A hybrid asymptotic-numerical technique is used to sum these infinite logarithmic expansions and obtain close agreement with full numerical results. The particular problems considered include viscous flow in a straight pipe and steady-state linear and nonlinear diffusion problems.

1 Introduction

In this paper we study elliptic problems in a two-dimensional domain that contains one or several small holes. The perturbing effect of the small holes is a singular perturbation in the sense that the holes produce large, but localized, changes in the solution. Hence the method of matched asymptotic expansions as described in Kevorkian & Cole [5] can be used to construct approximate solutions.

A critical feature of the problems that we consider is that the asymptotic solution involves an infinite logarithmic expansion in powers of $-1/\log\varepsilon$, where ε is a measure of the size of the perturbing subdomain. The difficulty of such asymptotic solutions is that when they converge they do so very slowly, meaning that a great number of terms in the expansion must be retained in order to have sufficient accuracy at moderately small values of the perturbation parameter ε. Lange & Weinitschke [7] examined strongly localized perturbations of elliptic problems on domains with small holes. In their study, they identified that reciprocal logarithmic expansions occur in such problems but they only calculated the leading-order term in the asymptotic solution. A hybrid asymptotic-numerical method was developed in Ward, Henshaw & Keller [15] to sum the infinite reciprocal logarithmic expansion occurring in the asymptotic solution to certain eigenvalue problems in two-dimensional domains with small holes. Subsequently, this method was applied to problems occurring in other disciplines including low Peclet number heat transfer (cf. Titcombe & Ward [13]) and low Reynolds number flow (cf. Kropinski, Ward & Keller [6]).

In this paper, we extend the previous analysis of the hybrid asymptotic-numerical method to treat other two-dimensional problems, including viscous flow in a straight pipe

[1]This work was supported by NSERC grant 5-81541. Email address: ward@math.ubc.ca

and certain linear diffusion problems. The mathematical model of fluid flow in a straight pipe involves Poisson's equation and its solution can be used to measure the viscosity of an unknown fluid. Shivakumar [12], Ward-Smith [14] and Piercy, Hooper & Whinny [10] considered problems of this type. Previous studies of steady-state diffusion problems, many of which are summarized in the treatises of Crank [4] and Carslaw & Jaeger [3], assume separable geometries so that eigenfunction expansion techniques or transform methods can be used to calculate the solution. We introduce perturbations to this type of geometry in two dimensions, which leads to the occurrence of infinite expansions of reciprocal logarithms and the need to sum the expansions. A physical interpretation of this type of diffusion problem is that of a pipe leaking material into the surrounding medium. Nithiarasu [9] and references therein contain details on the importance of other physical effects in this problem. Our present study of linear heat diffusion with no coupling to other physical effects is a first step in providing an analytical basis for studying these problems.

The outline of the paper is as follows. In §2 we use the hybrid method to analyze laminar fluid-flow in a pipe containing a thin core, and we compare the results with certain special analytical solutions and with full numerical solutions. In §3 we study a linear steady-state diffusion equation in a domain with several holes. Some examples of the theory are given. Finally, in §4 we show how the theory can be extended to treat nonlinear elliptic problems in two-dimensional domains with small holes.

2 Viscous Flow in a Straight Pipe with a Thin Core

We consider steady, incompressible, laminar flow in a straight pipe containing a thin core. Both the pipe and the core have a constant cross-section of arbitrary shape, and thus the problem is two-dimensional. With these assumptions, the pipe flow is unidirectional and the velocity component w in the axial direction satisfies

$$\triangle w = -\beta\,, \qquad \boldsymbol{x} \in D\backslash D^\varepsilon\,, \tag{2.1a}$$

$$w = 0\,, \qquad \boldsymbol{x} \in \partial D\,, \tag{2.1b}$$

$$w = 0\,, \qquad \boldsymbol{x} \in \partial D^\varepsilon\,. \tag{2.1c}$$

Here $D \in \mathcal{R}^2$ is the dimensionless pipe cross-section and D^ε is the cross-section of the thin core. We assume that D^ε has radius $O(\varepsilon)$ and that $D^\varepsilon \to \boldsymbol{\xi}$ uniformly as $\varepsilon \to 0$, where $\boldsymbol{\xi} \in D$. We denote the scaled subdomain that results from an $O(\varepsilon^{-1})$ magnification of the length scale of D^ε by $D_1 = \varepsilon^{-1} D^\varepsilon$. In (2.1a), β is determined in terms of the dynamic viscosity μ of the fluid and the pressure gradient dp/dz along the channel by

$$\beta = -\frac{1}{\mu}\frac{dp}{dz}\,. \tag{2.1d}$$

The well-know derivation of (2.1) is summarized in Appendix A.

In terms of w we can compute the mean flow velocity $\bar{w}$ as

$$\bar{w} = \frac{1}{A_D}\int_{D\backslash D^\varepsilon} w\, d\boldsymbol{x}\,. \tag{2.2}$$

Here A_D is the cross-sectional area of the pipe-core geometry. For laminar flow in pipes of non-circular cross-section, with or without cores, the friction coefficient f is expressed as (cf. [14])

$$f = \frac{16}{\mathrm{Re}} C_1 \equiv f_{cs} C_1 \,. \tag{2.3a}$$

Here $\mathrm{Re} = \bar{w} L \rho / \mu$ is the Reynolds number and ρ is the density of the fluid. Laminar flow occurs for Reynolds numbers in the approximate range $0 < \mathrm{Re} < 2000$. In (2.3a), $f_{cs} = 16/\mathrm{Re}$ is the friction coefficient for a pipe of circular cross-section without a core, and C_1 is a constant that depends on the pipe-core geometry. A collection of values of C_1 for various non-circular duct geometries appears in Table C5 of [14]. In the definition of Re, L is a characteristic diameter defined by $L = 4A_D/P_D$, where P_D is the wetted perimeter of the pipe and the core. The coefficient f can also be written as (see [14]):

$$f = \frac{-L(dp/dz)}{2\rho \bar{w}^2} \,. \tag{2.3b}$$

Substituting (2.3b) into (2.3a), and using the definition of β in (2.1d), we can express the constant C_1 as

$$C_1 = \frac{L^2 \beta}{32 \bar{w}} \,. \tag{2.3c}$$

Below, we will calculate $\bar{w}$ asymptotically and then compute C_1 in (2.3c) and compare to tabulated values in [14] for a special case of the pipe-core geometry.

The asymptotic solution to (2.1) is carried out in two different regions: an outer region defined at an $O(1)$ distance from the perturbing core and an inner region defined in an $O(\varepsilon)$ neighborhood of the thin core D^ε. In §2.1 we show how to calculate the sum of all the logarithmic terms for w, and in §2.2 we give some examples of the theory.

2.1 Summing the Logarithmic Expansion

In the outer region we expand the solution as

$$w(\boldsymbol{x}; \varepsilon) = W_0(\boldsymbol{x}; \nu) + \sigma(\varepsilon) W_1(\boldsymbol{x}) + \cdots \,. \tag{2.4}$$

Here $\nu = O(-1/\log \varepsilon)$ is a gauge function to be chosen, $\sigma \ll \nu$ as $\varepsilon \to 0$, and W_0 contains all of the logarithmic terms in the expansion. Substituting (2.4) into (2.1a) and (2.1b), and letting $D^\varepsilon \to \boldsymbol{\xi}$, we get

$$\triangle W_0 = -\beta \,, \qquad \boldsymbol{x} \in D \backslash \{\boldsymbol{\xi}\} \,, \tag{2.5a}$$

$$W_0 = 0 \,, \qquad \boldsymbol{x} \in \partial D \,, \tag{2.5b}$$

$$W_0 \quad \text{is singular as } \boldsymbol{x} \to \boldsymbol{\xi} \,. \tag{2.5c}$$

The matching of the outer and inner expansions will determine the singularity behavior for W_0 as $\boldsymbol{x} \to \boldsymbol{\xi}$.

In the inner region near D^ε we introduce the inner variables

$$\boldsymbol{y} = \varepsilon^{-1}(\boldsymbol{x} - \boldsymbol{\xi}), \qquad v(\boldsymbol{y};\varepsilon) = W(\boldsymbol{\xi} + \varepsilon\boldsymbol{y};\varepsilon). \tag{2.6}$$

If we naively assume that $v = O(1)$ in the inner region we obtain the leading order problem for v that $\triangle' v = 0$ outside D_1 with $v = 0$ on ∂D_1 and $v \to W_0(\boldsymbol{\xi})$ as $|\boldsymbol{y}| \to \infty$, where $\triangle'$ denotes the Laplacian in the $\boldsymbol{y}$ variable. The far-field condition as $|\boldsymbol{y}| \to \infty$ is obtained by matching v to the outer solution. However, in two-dimensions there is no solution to this problem since the Green's function for the Laplacian grows logarithmically at infinity. To overcome this difficulty, we require that $v = O(\nu)$ in the inner region and we allow v to be unbounded as $|\boldsymbol{y}| \to \infty$. Therefore, we expand v as

$$v(\boldsymbol{y};\varepsilon) = V_0(\boldsymbol{y};\nu) + \varepsilon V_1(\boldsymbol{y}) + \cdots, \tag{2.7a}$$

where we write V_0 in the form

$$V_0(\boldsymbol{y};\nu) = \nu\gamma v_c(\boldsymbol{y}). \tag{2.7b}$$

Here $\gamma = \gamma(\nu)$ is a constant to be determined with $\gamma = O(1)$ as $\nu \to 0$. Substituting (2.6) and (2.7) into (2.1a) and (2.1c), and allowing $v_c(\boldsymbol{y})$ to grow logarithmically at infinity, we get that $v_c(\boldsymbol{y})$ satisfies

$$\triangle' v_c = 0, \qquad \boldsymbol{y} \notin D_1, \tag{2.8a}$$

$$v_c = 0, \qquad \boldsymbol{y} \in \partial D_1, \tag{2.8b}$$

$$v_c \sim \log|\boldsymbol{y}|, \qquad |\boldsymbol{y}| \to \infty. \tag{2.8c}$$

The solution to (2.8) has the following far-field asymptotic behavior:

$$v_c(\boldsymbol{y}) \sim \log|\boldsymbol{y}| - \log d + O\left(\frac{1}{|\boldsymbol{y}|}\right), \qquad |\boldsymbol{y}| \gg 1. \tag{2.8d}$$

The constant $d > 0$, called the logarithmic capacitance, depends on the shape of D_1 but not on its orientation. Numerical values for d for different shapes are given in [11], and are reproduced in Table 1.

The leading order matching condition between the inner and outer solutions determines the constant γ in (2.7b). Writing (2.8d) in outer variables and substituting into (2.7b), we get the far-field behavior

$$v(\boldsymbol{y};\varepsilon) \sim \gamma\nu\left[\log|\boldsymbol{x} - \boldsymbol{\xi}| - \log(\varepsilon d)\right] + \cdots. \tag{2.9}$$

Choosing

$$\nu(\varepsilon) = -1/\log(\varepsilon d), \tag{2.10}$$

and matching (2.9) to the outer expansion (2.4) for W, we obtain the singularity condition for W_0,

$$W_0 = \gamma + \gamma\nu\log|\boldsymbol{x} - \boldsymbol{\xi}| + o(1), \quad \text{as} \quad \boldsymbol{x} \to \boldsymbol{\xi}. \tag{2.11}$$

D_1	d
circle, radius r	r
ellipse, semi-axes a and b	$\frac{a+b}{2}$
equilateral triangle, side h	$\frac{\sqrt{3}\,\Gamma\left(\frac{1}{3}\right)^3 h}{8\pi^2} \approx 0.422h$
isosceles right triangle, short side h	$\frac{3^{3/4}\Gamma\left(\frac{1}{4}\right)^2 h}{2^{7/2}\pi^{3/2}} \approx 0.476h$
square, side h	$\frac{\Gamma\left(\frac{1}{4}\right)^2 h}{4\pi^{3/2}} \approx 0.5902h$

Table 1: Shape-dependent parameter d for cross-sectional shape $D_1 = \varepsilon^{-1} D^\varepsilon$.

The solution to (2.5) together with (2.11) determines γ. This follows since for a singularity condition of the form $W_0 \sim S \log|\boldsymbol{x} - \boldsymbol{\xi}| + R$ for an elliptic equation, the constant R is not arbitrary but is determined as a function of S.

The solution for W_0 is decomposed as

$$W_0(\boldsymbol{x};\nu) = W_{0H}(\boldsymbol{x}) + 2\pi\gamma\nu G(\boldsymbol{x};\boldsymbol{\xi})\,. \tag{2.12}$$

Here $W_{0H}(\boldsymbol{x})$ is the smooth function satisfying the unperturbed problem

$$\triangle W_{0H} = -\beta\,, \qquad \boldsymbol{x} \in D\,, \tag{2.13a}$$

$$W_{0H} = 0\,, \qquad \boldsymbol{x} \in \partial D\,, \tag{2.13b}$$

and $G(\boldsymbol{x};\boldsymbol{\xi})$ is the Green's function satisfying

$$\triangle G = 0\,, \qquad \boldsymbol{x} \in D\backslash\{\boldsymbol{\xi}\}\,, \tag{2.14a}$$

$$G = 0\,, \qquad \boldsymbol{x} \in \partial D\,, \tag{2.14b}$$

$$G = \frac{1}{2\pi}\left[\log|\boldsymbol{x} - \boldsymbol{\xi}| + R(\boldsymbol{\xi})\right] + o(1)\,, \quad \text{as} \quad \boldsymbol{x} \to \boldsymbol{\xi}\,. \tag{2.14c}$$

Here $R(\boldsymbol{\xi})$ is the regular part of the Green's function at $\boldsymbol{x} = \boldsymbol{\xi}$, also know as the Robin constant (see [1]). Substituting (2.14c) into (2.12) and letting $\boldsymbol{x} \to \boldsymbol{\xi}$, we compare with (2.11) to obtain a formula for γ, which is

$$\gamma = \frac{W_{0H}(\boldsymbol{\xi})}{1 - \nu R(\boldsymbol{\xi})}\,. \tag{2.15}$$

Since $\beta > 0$ in (2.13a) we conclude from the maximum principle applied to (2.13) that $W_{0H}(\boldsymbol{\xi}) \neq 0$ for $\boldsymbol{\xi} \in D$. The range of validity of (2.15) is limited to values of ε for which $\nu R(\boldsymbol{\xi}) < 1$. This yields,

$$0 < \varepsilon < \varepsilon_c\,, \qquad \varepsilon_c \equiv \frac{1}{d}\exp\left[-R(\boldsymbol{\xi})\right]\,. \tag{2.16}$$

In summary, the inner and outer expansions that contain all of the logarithmic terms are given in the following result:

Proposition 2.1: *For $\varepsilon \ll 1$, the outer expansion for (2.1) is*

$$w \sim W_0(\boldsymbol{x};\nu) = W_{0H}(\boldsymbol{x}) + \frac{2\pi\nu W_{0H}(\boldsymbol{\xi})}{1-\nu R(\boldsymbol{\xi})} G(\boldsymbol{x};\boldsymbol{\xi})\,, \qquad |\boldsymbol{x}-\boldsymbol{\xi}| = O(1)\,, \tag{2.17a}$$

and the inner expansion with $\boldsymbol{y} = \varepsilon^{-1}(\boldsymbol{x}-\boldsymbol{\xi})$ is

$$w \sim V_0(\boldsymbol{y};\nu) = \frac{\nu W_{0H}(\boldsymbol{\xi})}{1-\nu R(\boldsymbol{\xi})} v_c(\boldsymbol{y})\,, \qquad |\boldsymbol{x}-\boldsymbol{\xi}| = O(\varepsilon)\,. \tag{2.17b}$$

Here $\nu = -1/\log[\varepsilon d]$, d is defined in (2.8d), $v_c(\boldsymbol{y})$ satisfies (2.8), W_{0H} satisfies the unperturbed problem (2.13), and $G(\boldsymbol{x};\boldsymbol{\xi})$ and $R(\boldsymbol{\xi})$ satisfy (2.14).

This formulation is referred to as the hybrid asymptotic-numerical method since it uses the asymptotic analysis as a means of reducing the original problem (2.1) with a hole to the simpler asymptotically related problem (2.5a), (2.5b) with singularity behavior (2.11). This related problem does not have a boundary layer structure and so is easy to solve numerically. The numerics required for the hybrid method involves the computation of the unperturbed solution W_{0H} and the Green's function $G(\boldsymbol{x};\boldsymbol{\xi})$. In terms of G we then identify its regular part $R(\boldsymbol{\xi})$. From the solution to the canonical inner problem (2.8) we then compute the shape parameter d. The result (2.17a) then shows that the asymptotic solution only depends on the product of εd and not on ε itself. This feature allows for an asymptotic equivalence between holes of different cross-sectional shape, based on an effective 'radius' of the cylinder. This equivalence is known as Kaplun's equivalence principle (cf. [6]).

An advantage of the hybrid method over the traditional method of matched asymptotic expansions is that the hybrid formulation is able to sum the infinite logarithmic series and thereby provide an accurate approximate solution. From another viewpoint, the hybrid problem is much easier to solve numerically than the full singularly perturbed problem (2.1). For the hybrid method a change of the shape of D_1 requires us, as a result of Kaplun's equivalence principle, to only re-calculate the constant d. This simplification does not occur in a full numerical approach.

2.2 Validation of the Hybrid Method

We compare the results of the hybrid method with results obtained either analytically or numerically from the full perturbed problem (2.1). We have used *Matlab* and its *Partial Differential Equations Toolbox* [8] for the direct numerical computations of solutions to (2.1). We indicate the direct numerical results as discrete points in the plots.

Example 2.1 (Concentric annulus): We consider flow between the walls of a circular pipe of radius r_0 and a concentric thin core of radius ε. Since the geometry is radially symmetric we have that $w = w(r;\varepsilon)$. In this case, we can solve (2.1) exactly to get

$$w_E = \frac{\beta}{4}\left[r_0^2 - r^2 - (r_0^2-\varepsilon^2)\frac{\log(r_0/r)}{\log(r_0/\varepsilon)}\right]. \tag{2.18}$$

Now, we consider the asymptotic solution for $w(r;\varepsilon)$ from the hybrid method. From (2.14), for a circular pipe of radius r_0 containing a core centered at $\boldsymbol{\xi} = \mathbf{0}$, the Green's function is

$$G = \frac{1}{2\pi}(\log r - \log r_0). \tag{2.19}$$

Thus, comparing with (2.14c), its regular part at the origin is $R(\mathbf{0}) = -\log r_0$. For a circular pipe of radius r_0, the solution to the unperturbed problem (2.13) is

$$W_{0H}(r) = \frac{\beta}{4}(r_0^2 - r^2)\,. \tag{2.20}$$

Thus, $W_{0H}(0) = \beta r_0^2/4$. In the case of a circular core, D^ε, of radius ε, the solution to (2.8) gives that the shape-dependent parameter is $d = 1$. Substituting all of this information into (2.15) we get

$$\gamma = \frac{\beta r_0^2}{4}\frac{\log\varepsilon}{\log(\varepsilon/r_0)}\,. \tag{2.21}$$

From (2.17a) we get that the hybrid solution, valid for $|\boldsymbol{x}| \gg O(\varepsilon)$, and correct to within all logarithmic terms, is

$$w(\boldsymbol{x};\varepsilon) = \frac{\beta}{4}\left[r_0^2 - r^2 - r_0^2\frac{\log(r_0/r)}{\log(r_0/\varepsilon)}\right]. \tag{2.22}$$

Comparing the exact solution in (2.18) with the hybrid solution in (2.22), we see that the hybrid method solution agrees well with the exact solution, except that the hybrid solution does not capture the $O(\varepsilon^2)$ term.

We compare the hybrid method results to those of the exact solution for the mean flow velocity $\bar{w}$ defined in (2.2). Using (2.18) in (2.2), the exact mean flow velocity $\bar{w}_E$ is

$$\bar{w}_E = \frac{\beta}{8}\left[r_0^2 + \varepsilon^2 - \frac{r_0^2 - \varepsilon^2}{\log(r_0/\varepsilon)}\right]. \tag{2.23}$$

In Fig. 1, for a concentric annulus with $r_0 = 2$ and $\beta = 1$, we have plotted the mean flow velocity $\bar{w}$ from (2.2) versus the core radius ε using the exact solution in (2.18) and the hybrid solution in (2.22). The range of ε in our plot lies well within the range of validity in (2.16). The plot indicates that the hybrid method results agree very well with the exact solution.

Using the mean flow velocity that we obtained from the hybrid method, we calculate the constant C_1 in (2.3a) and compare to tabulated values given in [14] of this constant for laminar flow through ducts of concentric annular section. Table 2 contains the hybrid method values and tabulated values of C_1 for several ratios of radii, ε/r_0. We see that for ratios of the radii of the pipe and core up to 0.01, the values of C_1 from the hybrid method are exactly the four-digit accurate tabulated values.

Example 2.2 (Concentric Annulus with Arbitrarily-Shaped Core): Next, we consider flow in a circular pipe D of radius $r_0 = 2$ that contains a concentric core D^ε

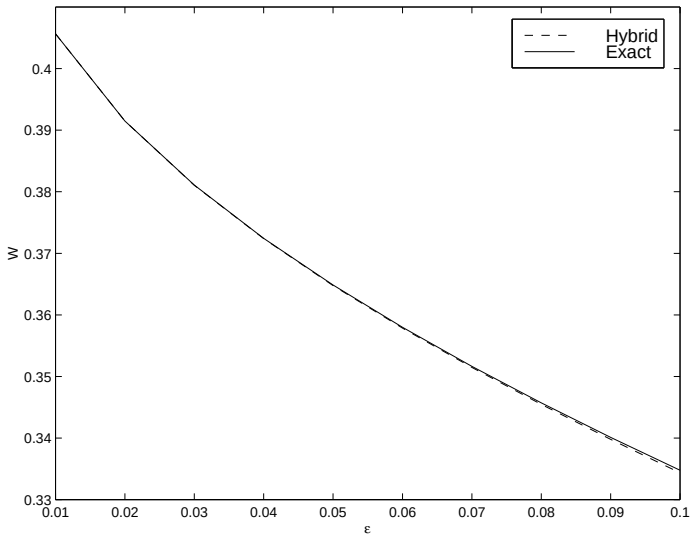

Figure 1: Mean flow velocity $\bar{w}$ versus pipe core radius ε for a concentric annulus $\varepsilon \leq r \leq 2$.

ε/r_0	Hybrid C_1	Tabulated C_1
0.0001	1.1216	1.1216
0.001	1.1669	1.1669
0.01	1.2518	1.2518
0.05	1.3496	1.3480
0.1	1.4065	1.3964
0.15	1.4554	1.4244

Table 2: Comparison of the constant C_1 in (2.3c) from the hybrid method solution with tabulated values of C_1 from [14] for laminar flow through ducts of concentric annular section.

of various cross-sectional shapes centered at the origin. We use Table 1 for the shape-dependent parameter d for a square core, an elliptic core, and an equilateral triangular core. Using the notation in the table, we set the major and minor semi-axes of the ellipse as $a = 2$ and $b = 1$, and both the side of the square and the equilateral triangle as $h = 1$. To compute the hybrid method solution, we use the Green's function in (2.19) and the unperturbed solution in (2.20) from the concentric annulus example since these solutions are independent of the shape and size of the core. The outer hybrid method solution is still given in (2.22) provided that we replace ε in (2.22) with εd. From this solution we then compute the asymptotic mean flow rate using (2.2).

To validate the asymptotic results for $\bar{w}$, we compared them with corresponding direct numerical results computed from the full problem (2.1) using the *Partial Differential Equations Toolbox* [8]. For a circular pipe of radius $r_0 = 2$ containing a concentric core and with $\beta = 1$, Fig. 2 contains curves of mean flow velocity, $\bar{w}$, versus ε, a measure of the size of the core, for three different cross-sectional shapes of the core. In the hybrid method solution, the change in shape and size of the core requires only that we vary the product εd, which

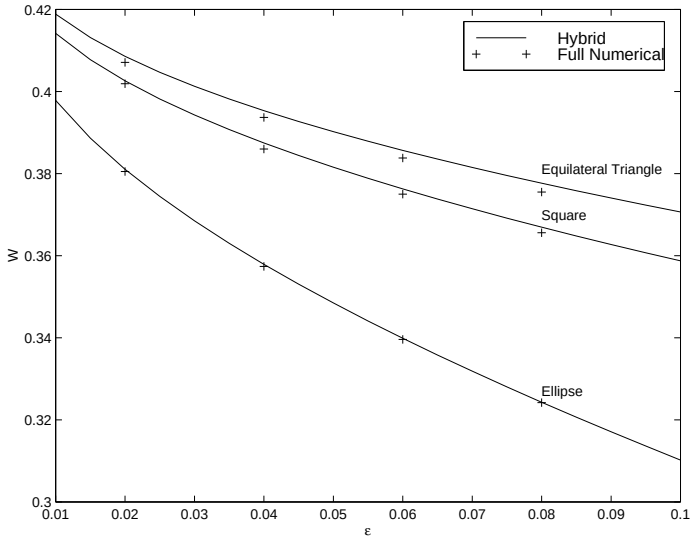

Figure 2: Hybrid method and direct numerical results for the mean flow velocity $\bar{w}$ versus measure of size ε of cross-sectional shape for a circular pipe of radius $r_0 = 2$ with a concentric core of three different cross-sectional shapes.

allows us to compute the entire ε curve very easily. In contrast, for each change of shape and size of the core in the direct numerical solution, we had to recreate the solution geometry and remesh the solution grid when using *Matlab*. For a core of elliptic cross-section, the figure shows that the hybrid method results agree very well with those of the direct numerical solution. The slight discrepancy in comparing the results for the other two core cross-sectional shapes, the square and equilateral triangle, could be due to the inability of the numerical method to resolve the corners of the core.

Example 2.3 (Eccentric Annulus): We consider flow in a circular pipe D of radius $r_0 > 1$ that contains a circular core D^ε of radius ε centered at $\boldsymbol{\xi} = (-1, 0)$.

From [14] and [10], the exact mean flow velocity $\bar{w}_E$ for this geometry is

$$\bar{w}_E = \frac{\pi\beta}{8A_D}\left[r_0^4 - \varepsilon^4 - \frac{4e^2M^2}{b-a} - 8e^2M^2\sum_{n=1}^{\infty}\frac{n\exp[-n(b+a)]}{\sinh[n(b-a)]}\right], \tag{2.24a}$$

where M, N, a and b are defined by

$$M = (N^2 - r_0^2)^{\frac{1}{2}}, \qquad N = \frac{r_0^2 - \varepsilon^2 + e^2}{2e}, \tag{2.24b}$$

$$a = \frac{1}{2}\log\left(\frac{N+M}{N-M}\right), \qquad b = \frac{1}{2}\log\left(\frac{N+M-e}{N-M-e}\right). \tag{2.24c}$$

Here $A_D = \pi(r_0^2 - \varepsilon^2)$ is the area of the pipe-core cross-section, and the eccentricity e is defined as the offset of the center of the subdomain D^ε from the center of D (see Fig. 3). Thus, $e = 1$ in our computations. A different method of solution, based on a complex variable method, was given in [12].

Now we calculate the terms in the hybrid solution given in (2.17). The unperturbed solution is again given in (2.20). The core is a circle of radius ε, so that the shape parameter

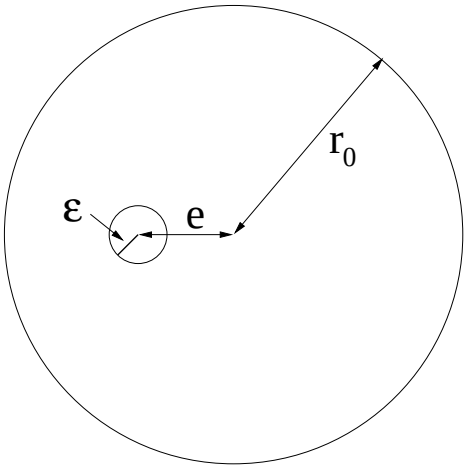

Figure 3: Geometry of the eccentric annular section of pipe and core.

is $d = 1$ and $\nu = -1/\log\varepsilon$. Next, using the method of images, we solve (2.14) analytically to obtain the Green's function

$$G(\boldsymbol{x};\boldsymbol{\xi}) = \frac{1}{2\pi}\log\left(\frac{|\boldsymbol{x}-\boldsymbol{\xi}|r_0}{|\boldsymbol{x}-\boldsymbol{\xi}'||\boldsymbol{\xi}|}\right) . \tag{2.25}$$

Here the image point $\boldsymbol{\xi}'$ of $\boldsymbol{\xi}$ in the circle of radius r_0 lies along the negative real axis and satisfies $|\boldsymbol{\xi}'||\boldsymbol{\xi}| = r_0^2$. Comparing (2.25) with (2.14c), we can then calculate the Robin constant $R(\boldsymbol{\xi})$ as

$$R(\boldsymbol{\xi}) = \log\left[\frac{r_0}{|\boldsymbol{\xi}-\boldsymbol{\xi}'||\boldsymbol{\xi}|}\right] . \tag{2.26}$$

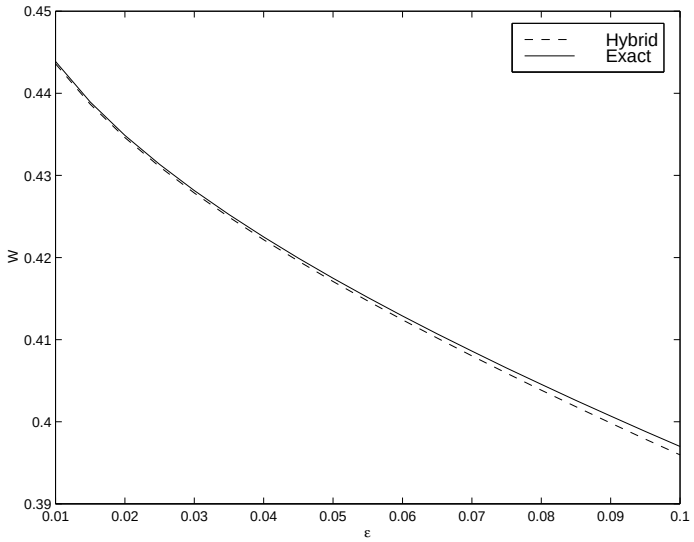

Figure 4: Mean flow velocity $\bar{w}$ versus pipe core radius ε for an eccentric annulus, with pipe radius $r_0 = 2$ and eccentricity $e = 1$.

Substituting (2.25), (2.26), $\nu = -1/\log\varepsilon$ and (2.20) into (2.17a) we obtain the outer solution for the hybrid method. This solution is then used in (2.2) with $A_D \sim \pi r_0^2$ to compute the mean flow velocity for the hybrid method. The integral in (2.2) is done using a numerical quadrature. In Fig. 4, for an eccentric annulus with pipe radius $r_0 = 2$ and with $\beta = 1$ and $e = 1$, we have plotted the mean flow velocity $\bar{w}$ versus the core radius ε from the exact solution and from the hybrid solution. For this example, the plot indicates that the hybrid method results compares quite well with the exact mean flow velocity.

We remark that for bodies of *arbitrary* shape centered at $\boldsymbol{\xi} = (-1, 0)$ the exact solution (2.24) does not apply. In this case, the hybrid method solution obtained above for the eccentric annulus still holds, provided that we replace $\nu = -1/\log\varepsilon$ in (2.17a) with $\nu = -1/\log[\varepsilon d]$, where d is to be computed from (2.8). In particular, if there is an ellipse with semi-axes ε and 2ε centered at $\boldsymbol{\xi} = (-1, 0)$ instead of the circle of radius ε, then from Table 1 we get $d = 3/2$. Hence, the plot in Fig. 4 for the hybrid solution still applies provided that we replace the horizontal axis in this figure by $3\varepsilon/2$.

3 Steady-State Diffusion in a Multiply-Connected Domain

For $\varepsilon \ll 1$, we consider the following singularly perturbed steady-state diffusion problem for $u(\boldsymbol{x};\varepsilon)$ in a domain $D \in \mathcal{R}^2$ that has N small holes:

$$\nabla\cdot[p(\boldsymbol{x})\nabla u] - m(\boldsymbol{x})u = 0\,, \qquad \boldsymbol{x} \in D\backslash\bigcup_{j=1}^{N} D_j^\varepsilon\,, \tag{3.1a}$$

$$\partial_n u + b(u - u_b) = 0\,, \qquad \boldsymbol{x} \in \partial D\,, \tag{3.1b}$$

$$u = \alpha_j\,, \qquad \boldsymbol{x} \in \partial D_j^\varepsilon\,, \qquad j = 1,\ldots,N\,. \tag{3.1c}$$

For simplicity we assume that α_j for $j = 1,\ldots,N$ are constants and that $p(\boldsymbol{x}) > 0$ and $m(\boldsymbol{x}) > 0$. In (3.1b), ∂_n denotes the outward normal derivative, $b > 0$ and u_b depends on $\boldsymbol{x} \in \partial D$. The subdomain D_j^ε of radius $O(\varepsilon)$, which models a localized sink or source of material, is strictly contained within D and the subdomains are assumed to be non-overlapping. We denote the scaled subdomain that results from an $O(\varepsilon^{-1})$ magnification of the length scale of D_j^ε by $D_j \equiv \varepsilon^{-1}D_j^\varepsilon$. Finally, we assume that $D_j^\varepsilon \to \boldsymbol{x}_j \in D$ uniformly as $\varepsilon \to 0$. A schematic plot of the geometry is shown in Fig. 5.

In §3.1 we construct an asymptotic solution to (3.1) that sums all of the logarithmic terms in the expansion of w, and in §3.2 we give some examples of the theory.

3.1 Summing the Logarithmic Series

In the *outer region*, defined away from D_j^ε for $j = 1,\ldots,N$, we expand

$$u(\boldsymbol{x};\varepsilon) \sim U_0(\boldsymbol{x};\boldsymbol{\nu}) + \sigma(\varepsilon)U_1(\boldsymbol{x}) + \cdots\,. \tag{3.2}$$

Here $\boldsymbol{\nu} = (\nu_1,\ldots,\nu_N)$ is a set of logarithmic gauge functions to be determined and $\sigma \ll \nu_j$ as $\varepsilon \to 0$ for $j = 1,\ldots,N$. Substituting (3.2) into (3.1a) and (3.1b), and letting $D_j^\varepsilon \to \boldsymbol{x}_j$

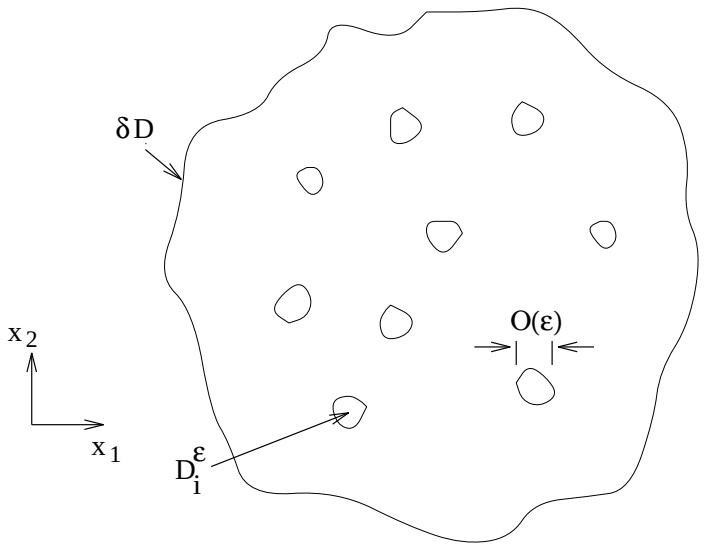

Figure 5: A schematic plot of the geometry of the singularly perturbed domain for (3.1). The domain D is assumed to have N small holes.

as $\varepsilon \to 0$, we get that

$$\nabla \cdot [p(\boldsymbol{x})\nabla U_0] - m(\boldsymbol{x})U_0 = 0\,, \qquad \boldsymbol{x} \in D\backslash\{\boldsymbol{x}_1, \ldots, \boldsymbol{x}_N\}\,, \tag{3.3a}$$

$$\partial_n U_0 + b\,(U_0 - u_b) = 0\,, \qquad \boldsymbol{x} \in \partial D\,, \tag{3.3b}$$

$$U_0 \quad \text{is singular as } \boldsymbol{x} \to \boldsymbol{x}_j\,, \quad j = 1, \ldots, N\,. \tag{3.3c}$$

The singularity behavior for U_0 as $\boldsymbol{x} \to \boldsymbol{x}_j$ will be found by matching the outer solution to the far-field behavior of the inner solution to be constructed near D_j^ε.

In the inner region near D_j^ε we introduce the inner variables $\boldsymbol{y}$ and $v(\boldsymbol{y};\varepsilon)$ by

$$\boldsymbol{y} = \varepsilon^{-1}(\boldsymbol{x} - \boldsymbol{x}_j)\,, \qquad v(\boldsymbol{y};\varepsilon) = u(\boldsymbol{x}_j + \varepsilon\boldsymbol{y};\varepsilon)\,. \tag{3.4}$$

In analogy with (2.7), we expand $v(\boldsymbol{y};\varepsilon)$ as

$$v(\boldsymbol{y};\varepsilon) = \alpha_j + \nu_j\gamma_j v_{cj}(\boldsymbol{y}) + \varepsilon V_{1j}(\boldsymbol{y}) + \cdots\,. \tag{3.5}$$

Here $\gamma_j = \gamma_j(\boldsymbol{\nu})$ is a constant to be determined and, as in (2.10), we choose

$$\nu_j = -1/\log[\varepsilon d_j]\,. \tag{3.6}$$

In analogy with (2.8), we get that $v_{cj}(\boldsymbol{y})$ satisfies

$$\triangle' v_{cj} = 0\,, \qquad \boldsymbol{y} \notin D_j\,, \tag{3.7a}$$

$$v_{cj} = 0\,, \qquad \boldsymbol{y} \in \partial D_j\,, \tag{3.7b}$$

$$v_{cj}(\boldsymbol{y}) \sim \log|\boldsymbol{y}| - \log d_j + O\left(\frac{1}{|\boldsymbol{y}|}\right)\,, \qquad |\boldsymbol{y}| \gg 1\,. \tag{3.7c}$$

Here d_j is determined by the shape of D_j.

Writing (3.7c) in outer variables and substituting the result into (3.5) we get the far-field expansion of v away from each D_j

$$v \sim \alpha_j + \gamma_j + \nu_j \gamma_j \log|\boldsymbol{x} - \boldsymbol{x}_j|\,, \qquad j = 1, \ldots, N\,. \tag{3.8}$$

Matching (3.8) to the outer expansion (3.2) we require that U_0 has the singular behavior

$$U_0 = \alpha_j + \gamma_j + \nu_j \gamma_j \log|\boldsymbol{x} - \boldsymbol{x}_j| + o(1)\,, \quad \text{as} \quad \boldsymbol{x} \to \boldsymbol{x}_j\,, \qquad j = 1, \ldots, N\,. \tag{3.9}$$

The solution to (3.3a) and (3.3b) together with (3.9) is decomposed as

$$U_0(\boldsymbol{x}; \boldsymbol{\nu}) = U_{0H}(\boldsymbol{x}) + 2\pi \sum_{k=1}^{N} \nu_k \gamma_k G(\boldsymbol{x}; \boldsymbol{x}_k)\,. \tag{3.10}$$

Here $U_{0H}(\boldsymbol{x})$ is the smooth function satisfying

$$\nabla \cdot [p(\boldsymbol{x}) \nabla U_{0H}] - m(\boldsymbol{x}) U_{0H} = 0\,, \qquad \boldsymbol{x} \in D\,, \tag{3.11a}$$

$$\partial_n U_{0H} + b\,(U_{0H} - u_b) = 0\,, \qquad \boldsymbol{x} \in \partial D\,, \tag{3.11b}$$

and $G(\boldsymbol{x}; \boldsymbol{\xi})$ is the Green's function satisfying

$$\nabla \cdot [p(\boldsymbol{x}) \nabla G] - m(\boldsymbol{x}) G = 0\,, \qquad \boldsymbol{x} \in D \backslash \{\boldsymbol{\xi}\}\,, \tag{3.12a}$$

$$\partial_n G + bG = 0\,, \qquad \boldsymbol{x} \in \partial D\,, \tag{3.12b}$$

$$G = \frac{1}{2\pi}\left[\log|\boldsymbol{x} - \boldsymbol{\xi}| + R(\boldsymbol{\xi})\right] + o(1)\,, \quad \text{as} \quad \boldsymbol{x} \to \boldsymbol{\xi}\,. \tag{3.12c}$$

Here $R = R(\boldsymbol{\xi})$ is the Robin constant for G.

Finally, to determine the γ_j we expand (3.10) as $\boldsymbol{x} \to \boldsymbol{x}_j$ to get

$$U_0 \sim U_{0H}(\boldsymbol{x}_j) + \nu_j \gamma_j \left[\log|\boldsymbol{x} - \boldsymbol{x}_j| + R(\boldsymbol{x}_j)\right] + 2\pi \sum_{\substack{k=1 \\ k \neq j}}^{N} \nu_k \gamma_k G(\boldsymbol{x}_j; \boldsymbol{x}_k)\,, \qquad j = 1, \ldots, N\,. \tag{3.13}$$

Comparing (3.13) with (3.9) we get the following linear system for the γ_j:

$$\gamma_j\left[-1 + \nu_j R(\boldsymbol{x}_j)\right] + 2\pi \sum_{\substack{k=1 \\ k \neq j}}^{N} \nu_k \gamma_k G(\boldsymbol{x}_j; \boldsymbol{x}_k) = \alpha_j - U_{0H}(\boldsymbol{x}_j)\,, \qquad j = 1, \ldots, N\,. \tag{3.14}$$

Here $\nu_j = -1/\log[\varepsilon d_j]$. In summary, the inner and outer expansions that contain all of the logarithmic terms are given in the following result:

Proposition 3.1: *For $\varepsilon \ll 1$, the outer expansion for (3.1) is*

$$u \sim U_0(\boldsymbol{x}; \boldsymbol{\nu}) = U_{0H}(\boldsymbol{x}) + 2\pi \sum_{k=1}^{N} \nu_k \gamma_k G(\boldsymbol{x}; \boldsymbol{x}_k)\,, \qquad |\boldsymbol{x} - \boldsymbol{x}_j| = O(1)\,, \tag{3.15a}$$

and the inner expansion near D_j^{ε} with $\boldsymbol{y} = \varepsilon^{-1}(\boldsymbol{x} - \boldsymbol{x}_j)$ is

$$u \sim \alpha_j + \nu_j \gamma_j v_{cj}(\boldsymbol{y})\,, \qquad |\boldsymbol{x} - \boldsymbol{x}_j| = O(\varepsilon)\,. \tag{3.15b}$$

Here $\nu_j = -1/\log[\varepsilon d_j]$, d_j is defined in (3.7c), $v_{cj}(\boldsymbol{y})$ satisfies (3.7), U_{0H} satisfies the unperturbed problem (3.11), and $G(\boldsymbol{x}; \boldsymbol{x}_j)$ and $R(\boldsymbol{x}_j)$ satisfy (3.12). Finally, the γ_j for $j = 1, \ldots, N$ are obtained from the linear system (3.14).

3.2 Some Examples of the Theory

In order to be able to determine most of the hybrid solutions analytically we shall assume in all of the examples below that $p(\boldsymbol{x}) \equiv 1$ and that $m(\boldsymbol{x}) \equiv 0$ or $m(\boldsymbol{x}) \equiv 1$, which yields either the reduced wave equation or the Laplacian, respectively. The terms needed in (3.15), apart for the shape-parameters d_j, can be determined explicitly provided that we can analytically calculate the unperturbed solution and the Green's function satisfying (3.11) and (3.12), respectively. When these analytical solutions are available, the hybrid method offers a tremendous advantage over a full numerical approach in that for the hybrid method one only needs to calculate the shape-parameters d_j numerically.

Example 3.1 (Circle Containing Small Holes with $m = 0$): Consider the following problem in the disk $D = \{r \mid 0 \le r \le 2\}$ that contains three small holes:

$$\triangle u = 0\,, \qquad \text{in} \quad D \backslash \bigcup_{j=1}^{3} D_j^{\varepsilon}\,, \tag{3.16a}$$

$$u = \alpha_j\,, \qquad \text{on} \quad \partial D_j^{\varepsilon}\,, \tag{3.16b}$$

$$u = 4\cos(2\theta)\,, \qquad \text{on} \quad |\boldsymbol{x}| = 2\,. \tag{3.16c}$$

We suppose that each of the holes has an elliptical shape with semi-axes ε and 2ε. Hence, from Table 1, the shape-parameter is $d = 3/2$ for each hole. As mentioned above, the orientation of the holes does not affect the asymptotic solution given in (3.15a). We assume that the holes are centered at $\boldsymbol{x}_1 = (1/2, 1/2)$, $\boldsymbol{x}_2 = (1/2, 0)$ and $\boldsymbol{x}_3 = (-1/4, 0)$. The boundary values on the holes are taken as $\alpha_1 = 1$, $\alpha_2 = 0$ and $\alpha_3 = 2$.

For this problem, the solution to the unperturbed problem (3.11) is

$$U_{0H}(x, y) = x^2 - y^2\,. \tag{3.17}$$

The Green's function, which is singular at $\boldsymbol{x}_j$, and the associated Robin constant, are calculated from the method of images as

$$G(\boldsymbol{x}; \boldsymbol{x}_j) = \frac{1}{2\pi} \log\left(\frac{|\boldsymbol{x} - \boldsymbol{x}_j|2}{|\boldsymbol{x} - \boldsymbol{x}_j'||\boldsymbol{x}_j|}\right)\,, \qquad R(\boldsymbol{x}_j) = \log\left[\frac{2}{|\boldsymbol{x}_j - \boldsymbol{x}_j'||\boldsymbol{x}_j|}\right]\,. \tag{3.18}$$

Here $\boldsymbol{x}_j'$ is the image point of $\boldsymbol{x}_j$ in the circle of radius 2. In this way, we get the numerical values

$$R(\boldsymbol{x}_1) = -0.5596\,, \qquad R(\boldsymbol{x}_2) = -0.6286\,, \qquad R(\boldsymbol{x}_3) = -0.6774\,. \tag{3.19}$$

Substituting (3.17), (3.18), (3.19) and $\nu = -1/\log(3\varepsilon/2)$ into (3.14), we obtain the following linear system for the γ_j:

$$\gamma_1\left[-1 - .5596\nu\right] + 2\pi\nu\left[\gamma_2 G(\boldsymbol{x}_1; \boldsymbol{x}_2) + \gamma_3 G(\boldsymbol{x}_1; \boldsymbol{x}_3)\right] = 1\,, \tag{3.20a}$$

$$\gamma_2\left[-1 - .6286\nu\right] + 2\pi\nu\left[\gamma_1 G(\boldsymbol{x}_2; \boldsymbol{x}_1) + \gamma_3 G(\boldsymbol{x}_2; \boldsymbol{x}_3)\right] = -1/4\,, \tag{3.20b}$$

$$\gamma_3\left[-1 - .6774\nu\right] + 2\pi\nu\left[\gamma_1 G(\boldsymbol{x}_3; \boldsymbol{x}_1) + \gamma_2 G(\boldsymbol{x}_3; \boldsymbol{x}_2)\right] = 31/16\,. \tag{3.20c}$$

After solving this linear system numerically for γ_j as a function of ε, the asymptotic outer solution is then given by substituting (3.17) and (3.18) into (3.15a). In Fig. 6 we plot the curves $\gamma_j(\varepsilon)$ as a function of ε. From this plot we observe that the leading order approximation to (3.20) valid for $\nu \ll 1$, which gives that $\gamma_1 = -1$, $\gamma_2 = 0.25$ and $\gamma_3 = -31/16$ is highly inaccurate even when ε is very small.

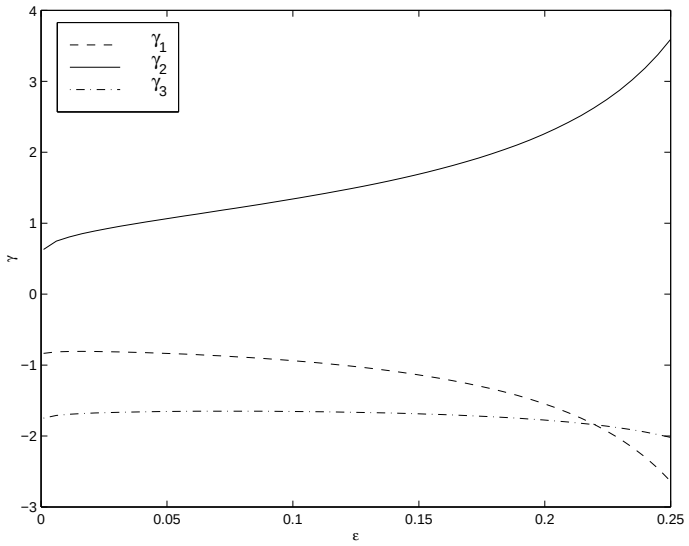

Figure 6: Plot of $\gamma_j = \gamma_j(\epsilon)$ for $j = 1, 2, 3$ obtained from the numerical solution to (3.20).

Example 3.2 (A Half-Space Problem): Consider the following problem in a half-space $D = \{(x, y) \,|\, -\infty < x < \infty,\ y \le 0\}$ that contains a small hole of arbitrary shape centered at some point $\boldsymbol{x}_1$ in the lower half- plane:

$$\triangle u - mu = 0\,, \qquad \text{in} \quad D\backslash D_1^\varepsilon\,, \tag{3.21a}$$

$$u = f(x)\,, \qquad \text{on} \quad y = 0\,, \tag{3.21b}$$

$$u = 1\,, \qquad \text{on} \quad \partial D_1^\varepsilon\,. \tag{3.21c}$$

Here $D_1^\varepsilon \to \boldsymbol{x}_1$ as $\varepsilon \to 0$. We label $\boldsymbol{x}_1 = (x_1, y_1)$ with $y_1 < 0$. In the notation of (3.15), $N = 1$ and $\alpha_1 = 1$. We will consider the two cases $m = 0$ and $m = 1$.

When $m = 1$, the unperturbed solution U_{0H} is

$$U_{0H}(x, y) = \frac{y}{\pi} \int_{-\infty}^{\infty} f(s) \left(\frac{K_0'\left([(s-x)^2 + y^2]^{1/2}\right)}{[(s-x)^2 + y^2]^{1/2}} \right) ds\,. \tag{3.22}$$

Using the method of images we can find the Green's function satisfying (3.12) as

$$G(\boldsymbol{x}; \boldsymbol{x}_1) = \frac{1}{2\pi} K_0\left(|\boldsymbol{x} - \boldsymbol{x}_1'|\right) - \frac{1}{2\pi} K_0\left(|\boldsymbol{x} - \boldsymbol{x}_1|\right)\,. \tag{3.23}$$

Here $\boldsymbol{x}_1' = (x_1, -y_1)$ is the reflection of $\boldsymbol{x}_1$ in the x-axis. Letting $\boldsymbol{x} \to \boldsymbol{x}_1$ in (3.23), we can identify the Robin constant in (3.12c) as

$$R(\boldsymbol{x}_1) = c - \log 2 + K_0\left(|\boldsymbol{x}_1 - \boldsymbol{x}_1'|\right)\,, \tag{3.24}$$

where c is Euler's constant. Hence, from (3.14),

$$\gamma_1 = \frac{U_{0H}(x_1, y_1) - 1}{1 - \nu_1 R(\boldsymbol{x}_1)}\,. \tag{3.25}$$

Substituting (3.22)–(3.25) and $\nu_1 = -1/\log[\varepsilon d_1]$ into (3.15a) determines the outer solution in terms of d_1 defined in (3.7).

Alternatively, when $m = 0$ we obtain readily that

$$U_{0H}(x, y) = -\frac{y}{\pi}\int_{-\infty}^{\infty} \frac{f(s)}{[(s-x)^2 + y^2]^{1/2}}\, ds\,. \tag{3.26}$$

The Green's function satisfying (3.12) is

$$G(\boldsymbol{x}; \boldsymbol{x}_1) = \frac{1}{2\pi}\left(\log|\boldsymbol{x} - \boldsymbol{x}_1| - \log|\boldsymbol{x} - \boldsymbol{x}_1'|\right)\,. \tag{3.27}$$

Letting $\boldsymbol{x} \to \boldsymbol{x}_1$ in (3.27), we can identify the Robin constant in (3.12c) as

$$R(\boldsymbol{x}_1) = -\log(2|y_1|)\,. \tag{3.28}$$

The formula for γ_1 is then given by (3.25), where U_{0H} and $R(\boldsymbol{x}_1)$ are defined in (3.26) and (3.28).

Example 3.3 (Circle Containing a Small Hole with $m = 1$): Consider the following problem in the disk $D = \{r \mid 0 \le r \le r_0\}$ that contains a small hole of arbitrary shape centered at $\boldsymbol{x}_1 \in D$:

$$\triangle u - u = 0\,, \qquad \text{in} \quad D\backslash D_1^\varepsilon\,, \tag{3.29a}$$

$$u = 1\,, \qquad \text{on} \quad r = r_0\,, \tag{3.29b}$$

$$u = 2\,, \qquad \text{on} \quad \partial D_1^\varepsilon\,. \tag{3.29c}$$

Here $D_1^\varepsilon \to \boldsymbol{x_1}$ as $\varepsilon \to 0$. We label $N = 1$ and $\alpha_1 = 2$ in the notation of (3.15). We will consider two different cases: a hole centered at the origin where $\boldsymbol{x}_1 = \boldsymbol{0}$ and an off-centered hole where $\boldsymbol{x}_1 \neq \boldsymbol{0}$.

We first consider the case where the hole is centered at the origin so that $\boldsymbol{x}_1 = \boldsymbol{0}$. Then, the unperturbed problem (3.11) and the Green's function problem (3.12) are radially symmetric. Solving these problems we get

$$U_{0H}(r) = \frac{I_0(r)}{I_0(r_0)}\,, \qquad G(r; \boldsymbol{0}) = -\frac{1}{2\pi}\left(K_0(r) - \frac{K_0(r_0)I_0(r)}{I_0(r_0)}\right)\,, \tag{3.30}$$

where $r = |\boldsymbol{x}|$. Here $K_0(r)$ and $I_0(r)$ are the usual modified Bessel functions. Using the asymptotic behavior $I_0(r) \sim 1$ and $K_0(r) \sim -\log r + \log 2 - c$ as $r \to 0$, where c is Euler's constant, we can expand G as $r \to 0$ to identify the Robin constant in (3.12c) as

$$R(\boldsymbol{0}) = c - \log 2 + \frac{K_0(r_0)}{I_0(r_0)}\,. \tag{3.31}$$

Substituting (3.30) and (3.31) into (3.14), we obtain γ_1 as

$$\gamma_1 = \frac{U_{0H}(0) - 2}{1 - \nu_1 R(\mathbf{0})}\,, \tag{3.32}$$

where $\nu_1 = -1/\log[\varepsilon d_1]$ and d_1 is defined in (3.7). Thus, from (3.15a), the asymptotic solution in the outer region is

$$u \sim U_{0H}(r) + 2\pi\nu_1 \left(\frac{U_{0H}(0) - 2}{1 - \nu_1 R(\mathbf{0})}\right) G(r;\mathbf{0})\,. \tag{3.33}$$

Table 1 can then be used to determine d_1 for various special shapes.

Next, consider an off-centered hole with $\boldsymbol{x}_1 \neq 0$. In this case, the unperturbed solution U_{0H} in (3.30) still applies, although we must compute the Green's function and the Robin constant numerically using *Matlab* (cf. [8]). As an example, suppose that the hole is centered at $\boldsymbol{x}_1 = (1/2, 1/2)$ and that $r_0 = 2$. Then, to compute $R(\boldsymbol{x}_1)$ numerically we first write G in terms of some function ψ as $G = (2\pi)^{-1}\left(\psi - K_0(|\boldsymbol{x} - \boldsymbol{x}_1|)\right)$. Then, ψ is smooth and satisfies $\triangle\psi - \psi = 0$ in $0 \leq |\boldsymbol{x}| \leq 2$ with $\psi = K_0\left(|\boldsymbol{x} - \boldsymbol{x}_1|\right)$ on $|\boldsymbol{x}| = 2$. Computing ψ numerically using *Matlab* we output $\psi(\boldsymbol{x}_1)$. The Robin constant is then given in terms of $\psi(\boldsymbol{x}_1)$ by

$$R(\boldsymbol{x}_1) = c - 2 + \psi(\boldsymbol{x}_1)\,, \tag{3.34}$$

where c is Euler's constant. In this way, we get the value $R(\boldsymbol{x}_1) = 0.773$. Defining $r_1 = |\boldsymbol{x}_1| = 1/\sqrt{2}$, we get from (3.14) that

$$\gamma_1 = \frac{U_{0H}(r_1) - 2}{1 - \nu_1 R(\boldsymbol{x}_1)}\,, \qquad R(\boldsymbol{x}_1) = 0.773\,. \tag{3.35}$$

Then in terms of a numerically computed Green's function the asymptotic outer solution can be obtained from (3.15a).

The examples described above only illustrate the hybrid method. There are many other geometries where the Green's function and the Robin constant can be found explicitly. In particular, they can be found for a quarter plane problem with $m = 0$ or $m = 1$ and for Laplace's equation in an infinite strip. In addition, they can be found for Laplace's equation whenever we can construct a conformal map $f(z)$ that takes the unperturbed domain to the unit circle.

4 A Class of Nonlinear Elliptic Problems

In this section we show how the method developed in §2 can be extended to treat nonlinear problems of the form

$$\triangle w + F(w) = 0\,, \qquad \boldsymbol{x} \in D\backslash D^{\varepsilon}\,, \tag{4.1a}$$

$$\partial_n w + b(w - w_b) = 0\,, \qquad \boldsymbol{x} \in \partial D\,, \tag{4.1b}$$

$$w = \alpha\,, \qquad \boldsymbol{x} \in \partial D^{\varepsilon}\,. \tag{4.1c}$$

Here α is constant, ∂_n denotes the outward normal derivative, $b > 0$, and D^ε is a small hole of radius $O(\varepsilon)$ with $D^\varepsilon \to \boldsymbol{\xi} \in D$ uniformly as $\varepsilon \to 0$. The function $F(w)$ is assumed to be smooth. The primary difference between the linear problem (2.1) and the nonlinear problem (4.1) is that the uniqueness and existence of solutions to the unperturbed problem corresponding to (4.1) may be a delicate issue. We shall assume that the unperturbed problem has at least one solution, and we will focus on determining how a specific solution to this problem is perturbed by the presence of the subdomain.

In the outer region we expand w as in (2.4). In analogy with (2.5), the leading term $W_0(\boldsymbol{x};\nu)$ in this expansion satisfies

$$\triangle W_0 + F(W_0) = 0\,, \qquad \boldsymbol{x} \in D\backslash\{\boldsymbol{\xi}\}\,, \tag{4.2a}$$

$$\partial_n W_0 + b(W_0 - w_b) = 0\,, \qquad \boldsymbol{x} \in \partial D\,, \tag{4.2b}$$

$$W_0 \quad \text{is singular as } \boldsymbol{x} \to \boldsymbol{\xi}\,. \tag{4.2c}$$

The analysis of the solution in the inner region is the same as in §2 since the effect of the nonlinear term in the inner region is at $O(\varepsilon^2)$, which is transcendentally small compared to the logarithmic terms. Hence, we require that W_0 has the following singular behavior as $\boldsymbol{x} \to \boldsymbol{\xi}$:

$$W_0 = \alpha + \gamma + \gamma\nu \log|\boldsymbol{x} - \boldsymbol{\xi}| + o(1)\,, \quad \text{as} \quad \boldsymbol{x} \to \boldsymbol{\xi}\,. \tag{4.3}$$

Here $\gamma = \gamma(\nu)$ is to be found and ν is defined in terms of the shape-parameter d by $\nu = -1/\log[\varepsilon d]$.

At this stage the asymptotic treatment of the nonlinear problem (4.1) differs from its linear counterpart (2.1). We suppose that for some range of the parameter S we can find a solution to (4.2a) and (4.2b) with the singular behavior

$$W_0 \sim S \log|\boldsymbol{x} - \boldsymbol{\xi}|\,, \quad \text{as} \quad \boldsymbol{x} \to \boldsymbol{\xi}\,. \tag{4.4}$$

Then, in terms of this solution we define the regular part $R = R(S;\boldsymbol{\xi})$ of W_0 by

$$R(S;\boldsymbol{\xi}) = \lim_{\boldsymbol{x}\to\boldsymbol{\xi}} \left(W_0 - S\log|\boldsymbol{x} - \boldsymbol{\xi}|\right)\,. \tag{4.5a}$$

Hence as $\boldsymbol{x} \to \boldsymbol{\xi}$ we have

$$W_0 = S\log|\boldsymbol{x} - \boldsymbol{\xi}| + R(S;\boldsymbol{\xi}) + o(1)\,. \tag{4.5b}$$

Equating (4.5b) to (4.3) we get $S = \nu\gamma$ and $R = \alpha + \gamma$, where $\nu = -1/\log[\varepsilon d]$. For fixed εd and α, these relations are two nonlinear algebraic equations for the two unknowns S and γ. Alternatively, we can view these relations as providing a parametric representation of the desired curve $\gamma = \gamma(\nu)$ in the form $\nu = \nu(S)$ and $\gamma = \gamma(S)$, where

$$\gamma = R(S;\boldsymbol{\xi}) - \alpha\,, \qquad \nu = \frac{S}{R(S;\boldsymbol{\xi}) - \alpha}\,. \tag{4.6}$$

Therefore, we can analytically sum all of the logarithmic terms in the expansion of the solution to (4.1) provided that we compute the regular part $R(S;\boldsymbol{\xi})$ of the singularity from the solution to (4.2a), (4.2b) with (4.4). In general this must be done numerically. However, we now illustrate the method with an example where we can calculate $R(S;\boldsymbol{\xi})$ analytically.

Example 4.1 (Concentric Annulus with Arbitrarily-Shaped Core): Let D be the unit ball, $b = \infty$, $w_b = 0$, $F(w) = e^w$, and assume that D^ε is centered at the origin. Then, (4.2a), (4.2b) and (4.4) yield the following problem for the radially symmetric function $W_0(r)$:

$$W_0'' + \frac{1}{r}W_0' + e^{W_0} = 0\,, \qquad 0 < r \le 1\,, \tag{4.7a}$$

$$W_0 = 0\,, \qquad \text{on} \quad r = 1\,, \tag{4.7b}$$

$$W_0 \sim S\log r\,, \qquad \text{as} \quad r \to 0\,. \tag{4.7c}$$

To solve this problem analytically, we introduce the new variables v and η defined by

$$v = W_0 - S\log r\,, \qquad \eta = r^{1+S/2}\,. \tag{4.8}$$

When $S > -2$, we then obtain that $v = v(\eta)$ is smooth and satisfies

$$v'' + \frac{1}{\eta}v' + \left(1+\frac{S}{2}\right)^{-2} e^v = 0\,, \qquad 0 \le \eta \le 1\,, \tag{4.9a}$$

$$v = 0\,, \qquad \text{on} \quad \eta = 1\,. \tag{4.9b}$$

The well-known solution to (4.9) can be written in parametric form as (cf. [2])

$$v(\eta) = 2\log\left(\frac{1+\rho}{1+\rho\eta^2}\right)\,, \tag{4.10a}$$

where $\rho = \rho(S)$ is given by

$$\left(1+\frac{S}{2}\right)^{-2} = \frac{8\rho}{(1+\rho)^2}\,. \tag{4.10b}$$

The maximum of the right side of (4.10b) is 2 and occurs when $\rho = 1$. Hence, for there to be a solution to (4.7) we require that $(1+S/2)^2 > 1/2$, which yields that $S > \sqrt{2}-2$. When $S > \sqrt{2}-2$, (4.10b) has two roots for ρ and hence (4.7) has two solutions. Let's consider the solution with the smaller root, which we label by ρ_-. Then, we calculate that

$$\rho_-(S) = (S+1)(S+3) - (S+2)\left[(S+2)^2 - 2\right]^{1/2}\,. \tag{4.11}$$

Setting $\eta = 0$ in (4.10a), and using (4.8), we compare with (4.5a) to conclude that $R(S;\mathbf{0}) = v(0)$, which yields

$$R(S;\mathbf{0}) = 2\log(1+S/2) + \log\left[8\rho_-(S)\right]\,. \tag{4.12}$$

Substituting (4.12) into (4.6) gives a parametric representation of the curve $\gamma = \gamma(\nu)$ in the form $\nu = \nu(S)$ and $\gamma = \gamma(S)$.

A Derivation of Pipe Flow Equation

The derivation of (2.1) begins with the Navier-Stokes equations for steady, incompressible flow in three dimensions

$$\rho(\boldsymbol{u}\cdot\nabla)\boldsymbol{u}+\nabla p=\mu\Delta\boldsymbol{u}\,, \tag{A.1a}$$

$$\nabla\cdot\boldsymbol{u}=0\,. \tag{A.1b}$$

Here $\boldsymbol{u}=(u,v,w)$ is the velocity vector, ρ the density, μ the dynamic viscosity, and p is the pressure of the fluid. Both $\boldsymbol{u}$ and p are functions of $\boldsymbol{x}=(x,y,z)$. The boundary conditions are that $\boldsymbol{u}=\boldsymbol{0}$ on the pipe and the core walls. We orient the reference frame so that the positive z-direction is along the axis of the pipe in the direction of the flow. With our assumptions, the pipe flow is unidirectional and hence, the velocity vector has the form $\boldsymbol{u}=(0,0,w)$. Then, (A.1b) gives that $\partial w/\partial z=0$ and so $w=w(x,y)$. From the x- and y-momentum equations, obtained from (A.1a), we get that $p=p(z)$. The z-momentum equation of (A.1a) then reduces to the two-dimensional equation

$$\frac{1}{\mu}\frac{dp}{dz}=\frac{\partial^2 w}{\partial x^2}+\frac{\partial^2 w}{\partial y^2}. \tag{A.2}$$

Since the left-hand side of this equation is a function of z only and the right-hand side is a function of (x,y) only, we can equate both sides to a constant. Thus, we define the positive constant β by

$$\beta=-\frac{1}{\mu}\frac{dp}{dz}\,. \tag{A.3}$$

The boundary conditions for w in (2.1b) and (2.1c) are that the axial flow velocity vanish on the boundaries of the pipe and the thin core.

References

[1] C. Bandle, M. Flucher, *Harmonic Radius and Concentration of Energy; Hyperbolic Radius and Liouville's Equation*, SIAM Review **38**, No. 2, (1996), pp. 191–238.

[2] J. D. Buckmaster, G. S. Ludford, *Theory of Laminar Flames*, Cambridge Univ. Press, Cambridge, (1982).

[3] H. S. Carslaw, J. C. Jaeger, *Conduction of Heat in Solids*, Clarendon Press, Oxford, (1959).

[4] J. Crank, *The Mathematics of Diffusion*, Oxford Science Publications, Clarendon Press, Oxford, (1983).

[5] J. Kevorkian, J. Cole, *Multiple Scale and Singular Perturbation Methods*, Applied Mathematical Sciences 114, Springer-Verlag, New York, (1996).

[6] M. C. Kropinski, M. J. Ward, J. B. Keller, *A Hybrid Asymptotic-Numerical Method for Calculating Low Reynolds Number Flows Past Symmetric Cylindrical Bodies*, SIAM J. Appl. Math. **55**, No. 6, (1995), pp. 1484–1510.

[7] C. Lange, H. Weinitschke, *Singular Perturbations of Elliptic Problems on Domains with Small Holes*, Studies in Appl. Math. **92**, (1994), pp. 55–93.

[8] MathWorks, Inc. *Partial Differential Equations Toolbox, User's Guide.* MATLAB. The MathWorks, Inc., Natick, Mass., (1996).

[9] P. Nithiarasu, *Finite Element Modeling of a Leaking Third Component Migration from a Heat Source Buried into a Fluid Saturated Porous Medium*, Math. and Comp. Modeling, **29**, (1999), pp. 27–39.

[10] N. A. V. Piercy, M. S. Hooper, H. F. Winny, *Viscous Flow Through Pipes with Cores*, Phil. Magazine, **15**, No. 7, (1933), pp. 647–676.

[11] T. Ranford, *Potential Theory in the Complex Plane*, Vol. 28 of London Mathematical Society Student Texts, Cambridge University Press, (1995).

[12] P. N. Shivakumar, C. Ji, *On the Poisson's Equation for Doubly Connected Regions*, Canadian Appl. Math. Quarterly, **1**, No. 4, (1993), pp. 555–568.

[13] M. Titcombe, M. J. Ward, *Convective Heat Transfer Past Small Cylindrical Bodies*, Studies in Appl. Math. **91**, (1997), pp. 81–105.

[14] A. J. Ward-Smith, *Internal Fluid Flow*, Clarendon Press, Oxford, United Kingdom, (1980).

[15] M. J. Ward, W. D. Henshaw, J. B. Keller, *Summing Logarithmic Expansions for Singularly Perturbed Eigenvalue Problems*, SIAM J. Appl. Math. **53**, No. 3, (1993), pp. 799–828.